Egypt.J.Chem. **Vol. 63**, No.6 . pp. 2051- 2062 (2020)

Egyptian Journal of Chemistry
http://ejchem.journals.ekb.eg/

Utilization of Nano-Black Sand as Filler in Styrene Butadiene Rubber Composites

S. N. Lawandy[1], R. Sayed[2], B. K. Saleh[1]*, S. F. Halim[1]
[1] *Polymer Metrology and Technology Lab., National Institute of Standards, Egypt.*
[2] *Nanotechnology and Nanometrology Lab., National Institute of Standards, Egypt.*

BLACK sand (BS) was obtained from Rozita Beach in Egypt. It processed, for the first time, to reach the nanoscale range using Ball Mill technique. Different techniques were used to examine the BS nanoparticles (BS-NPs) including XRD and TEM. XRD analyses showed that BS-NPs composed mainly of Albite (Sodium Aluminium Silicate) up to 64% approximately. Silicon dioxide and zirconium oxide are also included in lower amounts 17.7 and 18.5 %, respectively. TEM examinations indicated that BS-NPs size ranged from 6 to 122 nm and the main diameter value was 31 nm. Novel polymeric nanocomposites were prepared by incorporating different concentrations of BS nanoparticles (BS-NPs) in Styrene butadiene rubber (SBR) matrix. The role of BS-NPs as filler was evaluated in terms of the rheometeric and mechanical properties of the SBR/BS nanocomposites. Compression technique was used to access the crosslink density of the nanocomposites. In parallel, SBR compounds containing carbon black and nanosilica, as fillers, were studied for comparison. Cure and mechanical measurements indicated that cure characteristics somehow approached those of NSPs and tensile poperties were founf to be close in value to those of SBR-NSPs canocomposites.

Keywords: Black Sand nanoparticles, SBR nanocomposites, XRD, HR-TEM, Cure and mechanical properties.

Introduction

The preparation of polymeric nanocomposite filled with inorganic nanoparticles has been of great interest for both academic researches and industrial applications. A wide variety of inorganic materials has been used in polymer nanocomposites [1]. Among them, silica is the most studied material. The hybrid structures of silica/polymer have excellent physical reinforcement, high thermal resistance, high flexibility, high gas permeability and low surface energy [2, 3].

Egyptian black sand (BS) deposits occur mainly in four localities namely, the beach areas of Rosetta, Damietta, north Sinai, and the coastal sand dunes of El Burullus-Baltim [4]. In literature, the Egyptian black sand (BS) deposits were subjected to extensive research which dealt mainly with the mineralogy of these black sands and discussion of their economics [5]. Many studies stated that the Egyptian black sand deposits comprise huge reserves of certain economic mineral, for example, zircon (ZrSiO4) [6], rutile (TiO2) [7], ilmenite (Fe2+TiO_3) [8], and garnet ($X_3Y_2Si_3O_{12}$) where X-Mg, Fe, Ca and Y-Al, Fe, Cr) [9]. However, the average content of total economic minerals differs from place to other along the northern coast of Egypt [10].

The objective of the present study is to take advantage of the sand nature collected from the beach area of Rosetta area and use it, for the first time, as a filler to tailor styrene-butadiene polymeric nanocomposites. Ball mill was utilized to process BS particles to the nanoscale range, because it is an effective technique to produce nanoparticles [12]. Also, it has been shown to modify the filler morphology, which enhances the compatibility of fillers with polymer blends [13].

*Corresponding author e-mail: basmasalehnis@yahoo.com
Received 9/8/2019; Accepted 4/12/2019
DOI: 10.21608/ejchem.2019.15839.1958

Experimental

Materials and Methods

BS samples were collected, using a plastic cup, from the beach area of *Rosetta*, *Egypt*›s Beheira Governorate. They were selected from the upper 10 cm layer of the sea shore and then stored in plastic bags. The collected BS samples were sieved to remove coarse particles then dried in an air vacuum oven. A laboratory ball milling machine used to reduce the sand particle size to the nanoscale. Styrene butadiene rubber (SBR), trade name- Buna SE 1502 L supplied by ARLANXEO Deutschland GmbH, Business Unit Tire & Specialty. Zinc oxide and stearic acid were added to the SBR gum at first as plasticizers. Curing system comprises from N-cyclohexyl benzthiazyl sulfonamide (CBS), diphenyl guanidine (DPG) and sulfur (S) was added. Diphenyl guanidine (DPG) accelerator was used to accelerate curing process. 2-Mercaptobenzimidazole (MB) was used as antioxidant. To evaluate the role of BS-NPs as a filler in the SBR composites, SBR compounds containing high abrasion furnace black (HAF-N330), with mean particle size 32 nm and nanosilica (NS) with mean particle size 12 nm were prepared. The formulations of the different SBR composites are given in Table (1).

Preparation of BS-NPs/SBR nanocomposites

The black sand nanoparticles/SBR rubber (BS-NPs/SBR) nanocomposites were compounded using laboratory two-roll mill (152.4 × 330.2 mm) at a gear ratio 1:1.4. The nip gap, roll speed ratio, and number of passes were kept the same for all of the mixes. Firstly, the SBR matrix was masticated on a two-roll mill. Then different types of fillers along with different concentrations of BS-NPs were added to the SBR matrix followed by other ingredients according to ASTM D-3182-16. Different mix formulations are given in table 1.

Cure characteristics and samples preparation

The rheometeric properties were determined with an oscillating disk rheometer (Alpha Technologies MDR 2000) working at 170°C for 30 minute. The cure characteristics of the different mixes maximum torque (MH), minimum torque (ML), scorch time ts_2 (a measure of premature vulcanization of rubber) and the optimum cure time (Tc_{90}) time required to reach 90% crosslinking) were recorded. Delta torque ($\Delta M = M_H - M_L$) and Cure rate index (CRI= $100/tc_{90} - ts_2$) were calculated. Sheet samples for testing were compression molded in a laboratory hydraulic press (Mackey Bowley, C1136199) at 170°C at a pressure of 13.5 MPa according to ASTM D2084-17. The prepared nanocomposites were molded to the optimum cure, using molding conditions that were previously determined from rheometer data. Dumbbell shape samples of thickness 2.5 mm were cut from the compressed sheets using standard cutter according to ASTM D 412-16.

Characteristics

X-Ray Diffraction

X-Ray Diffractometry (XRD) analysis for powder of milled BS was carried out using BRUKER- D8 Advance X-ray diffractometer with Cu-Kα (λ=1.54A_o) as a radiation source, operating voltage at 45 kV and current 40 mA. The pattern is recorded in the wide angle range from 4^0 to 80^0 with step 0.02^0.

TABLE 1. Formulations of different SBR-filler compounds.

Ingredients, phr	Bo	B1	B2	B3	B4	B5
SBR	100	100	100	100	100	100
Processing Oil	5	5	5	5	5	5
Paraffin Wax	2	2	2	2	2	2
Zinc Oxide	3	3	3	3	3	3
Stearic Acid	2	2	2	2	2	2
MB	1.5	1.5	1.5	1.5	1.5	1.5
CBS	0.75	0.75	0.75	0.75	0.75	0.75
DPG	0.25	0.25	0.25	0.25	0.25	0.25
Sulfur	2.5	2.5	2.5	2.5	2.5	2.5
HAF-N 330	--	5	--	--	--	--
Nanosilica (NS)	--	--	5	--	--	--
Black Sand (BS-NPs)	--	--	--	5	10	15

FT-IR Spectroscopy

A Nicolet 380 thermo Fourier transform infrared (FITR) spectrometer with an attenuated total reflection (ATR) accessory and a zinc selenide crystal was used to analyze the BS-NPs sample. Scans were obtained with a resolution of 4 cm^{-1}.

HR-TEM studies

To estimate the particle size of BS-NPs, a sample was imaged by high resolution transmission electron microscope (HR-TEM, Jeol JEM 2100, Japan) operated at 200 Kev. The sample was prepared by dispersing it in methane. This dispersion is then dropped on carbon copper grids.

Mechanical properties

For measuring the mechanical properties of the rubber vulcanizates, sheets of dimensions 230 mm × 230 mm × 2.8 mm were prepared using a hydraulic press under a pressure of 150 kg/cm^2. Dumbbell shaped samples were cut from the molded sheets. Modulus, tensile strength and elongation at break were determined using a Zwick (Germany) tensile testing machine (Model Z010) at a temperature of 23 ± 200 C and a crosshead speed of 500 mm/min according to ASTM D412-16.

Compression measurements

The compression-recovery measurements were used to determine the compression and recovery percentage from which the crosslink density was evaluated.

Compression-recovery measurements

Cylindrical samples of dimension 22 mm diameter and 10 mm thickness were molded in the hydraulic press at the same conditions of temperature and time recorded before by the rheometer. A compression set device was used to accommodate all samples at the same time. The device consists of four steel plates between which the samples are compressed. The plates are held together by three axial bolts. Ring- shaped spacers of different thickness, 6.00, 7.614 and 9.228 mm, are placed around three axial bolts [14]. The different thicknesses (ls) of the spacers help to control the degree of compression. After placing the samples in between the steel plates, the bolts were tightened firmly over the samples. The compression set, including the samples, was accommodated in an air circulating oven at 70°C for 48 hours. After then, it is removed from the oven and allowed the whole set to cool. Then, the samples were released and allowed to recover for half an hour before measuring the final thickness accurately. The compression and recovery percentage was calculated using the following relations,

$$\text{Compression}, \% = \frac{lo - ls}{l0} \times 100 \quad (1)$$

$$\text{Recovery}, \% = \frac{lo - lr}{lo - ls} \times 100 \quad (2)$$

where, ***lo*** is the sample initial thickness, ***lr*** is the sample thickness after recovery and ***lr*** is the spacer thickness.

Crosslink density determinations

The physical crosslink density of various styrene butadiene and nitrile rubber compounds was estimated using the Kinetic Theory of Elasticity [15, 16]. The theory relates the force F applied per unit area A required to strain a perfectly elastic network at a small extension ratio, λ, by the following equations:

$$\frac{F}{A_0} = \frac{\rho RT}{Mc} (\lambda - \lambda^{-2}) \; dyne.cm^{-2} \quad (3)$$

$$M_c = \frac{\rho RT A_0}{F} (\lambda - \lambda^{-2}) \quad g/mole^{-1} \quad (4)$$

where, ρ is the density of rubber, T is the absolute temperature, R is Boltzman's constant, and M_c is molecular weight between two crosslinks. The crosslink density was expressed in terms of M_c as follows:

$$\nu = \frac{1}{2Mc} \; g^{-1}.mol \quad (5)$$

In the stress strain measurements the extension ratio λ is defined as l/l_0, where l_0 and l are the specimen thickness before and after strain respectively. In this study the force applied on the sample F/A_0 was compression stress and was calculated as follows:

$$F/A\_(0) = (\text{compression}\,\% \times 1000 \times 981)/(\pi r \wedge 2) \quad (6)$$

where, r is the radius of the compressed sample. The values of F/A_0 obtained from the Equation 4, for each sample, were plotted versus the values of $\lambda - \lambda^{-2}$, where λ here is defined as l_0/l_r instead of l/l_0. Results of these calculations are illustrated in Figure (1) where the slope of the straight line gives the value of $\frac{\rho RT}{Mc}$. Thus the Mc values of each sample were calculated and subsequently the cross link density by using Equation (5). It is to be noted here that there is a limit of 30% compression. For compression greater than 30% the

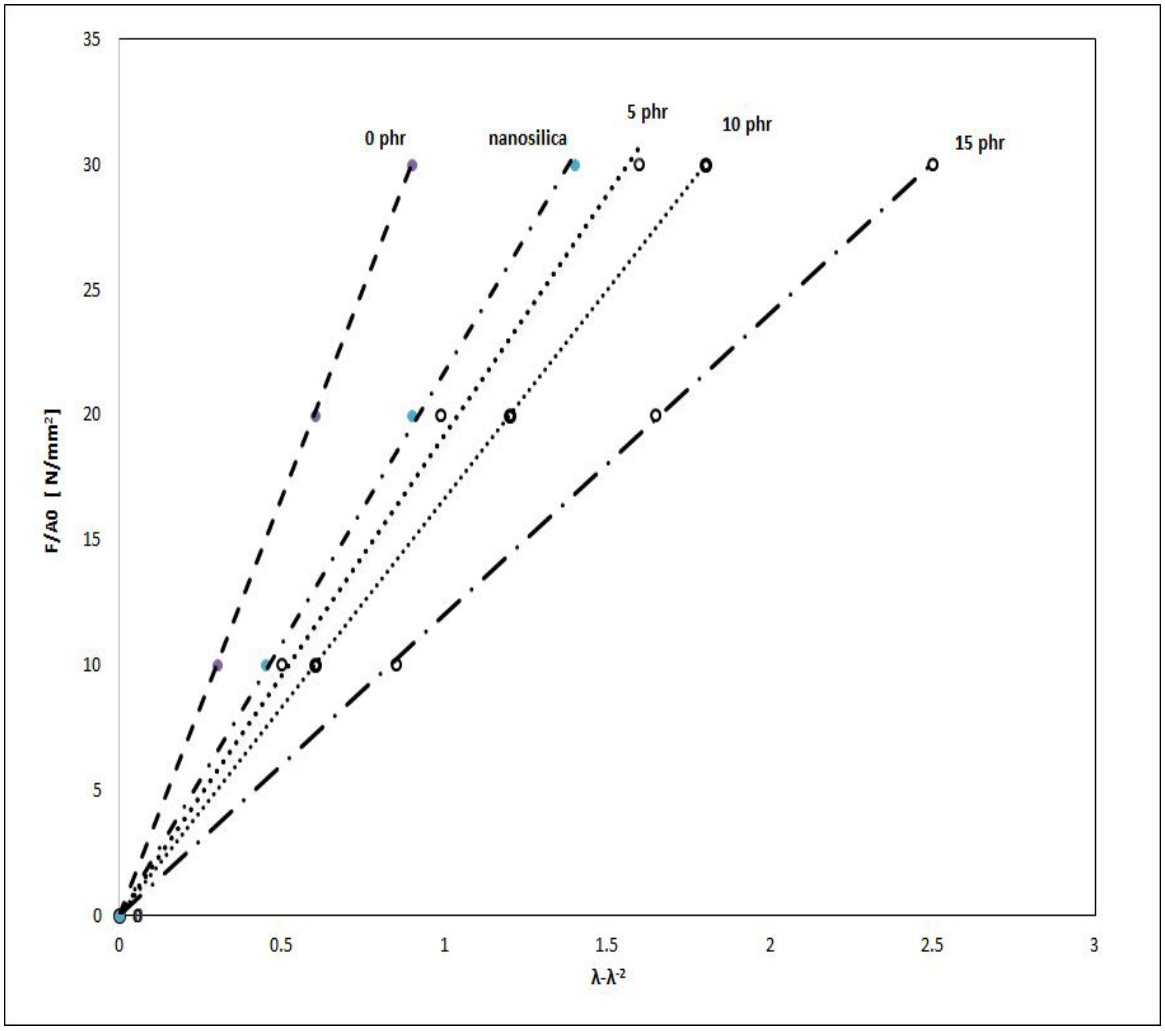

Fig. 1. Relationship between force applied on SBR/filler nanocomposites versus $\lambda-\lambda^{-2}$.

values were far from linearity; in other words do not obey the statistical theory of elasticity.

Hardness

Hardness testing measurements were carried out according to ASTM D 2240-15. Hardness determination was made using a Zwick Hardness Tester 3150, Germany. Test specimens used were cylindrical in shape with thickness and diameter 6.00 ± 0.2 mm and 14.00 ± 0.2 mm respectively.

Results and Discussions

BS-NPs Characterization

The size of the BS-NPs particles was examined by HR-TEM. Figure (2) showes that the BS-NPs particles are not uniform with agglomeration among them. Nanoparticles agglomeration usually happens to be due to the extreme small dimensions and high surface energy [17, 18]. Figure (3) represents particle size histogram, the nano-crystalline particles size of BS-NPs ranged from 6 to 122 nm and the mean diameter is about 31 nm.

Structural determination and estimation of crystallite size of the BS-NPs were characterized by XRD. The diffraction pattern is recorded in the wide angle range from 4^0 to 80^0 with step 0.02^0, as shown in Figure (4). The XRD patterns were analyzed and indexed using ICDD (International Center for Diffraction Data) data base. These data are given in Table (2). XRD examination demonstrates that the BS-NPs contain quartz (SiO_2), Albite ($NaAlSi_3O_8$) and baddeleyite (ZrO_2) in the ratio 17.7, 63.8 and 18.5 by weight respectively. Each of these minerals has its own crystalline structure. The variety in

the crystal structure is suggested to be a privilege for the BS-NPs to act as filler in the polymeric composites. This can be attributed to the fact that albite is a superior substitute for alumina and SiC is a reinforcing material in metal matrix composites [19, 20]. Moreover the monoclinic crystal lattice structure of baddeleyite has small grain size and non-spherical crystal shape yield high surface to volume ratios [21].

The FTIR measurements support the XRD results that demonstrate the existence of different minerals in BS-NPs. The FTIR spectrum is shown in Figure (5). The characteristic feature of quartz is the doublet appearing at 777 cm^{-1} and 795 cm^{-1} due to Si-O symmetrical stretching vibration. Moreover, the peaks at wavelength 459.6 cm^{-1} (Si-O asymmetrical bending vibrations), 694.4 cm^{-1} (Si-O symmetrical bending vibrations) are ascribed to existence of quartz in the samples [22]. The broad band at 3852.9 $cm^{-1}$and the peak placed at 1619.4 cm^{-1} referred to the H-O-H stretching and bending modes of the adsorbed water respectively, related to the silanol OH groups (20).The deformation vibrations of Al-O-Si and Si-O-Si are allocated in the region 530 $cm^{-1}$and 483 cm^{-1}, respectively [23]. The broad band at 1080 cm^{-1} is probably due to Si-O-Si symmetrical vibration or to the Zirconyl bonds Zr = O (11).The observed absorption peak at about 470 cm^{-1} region is due to the Zr–O vibration, which confirms the formation of ZrO_2 structure. However, weak peaks in the range 460 cm^{-1} to 690 cm^{-1} corresponding to monoclinic ZrO_2 are observed. A similar observation was reported by Chen et al. [24] for zirconia nanoparticles.

BS-NPs/ SBR Composites Properties

The present study comprises of two criteria a) compare the effect of BS-NPs with other fillers, with different structure and particle sizes, on the SBR properties; b) study of the effect of different concentrations of BS-NPs on the SBR/ BS-NPs nanocomposites.

Rheometric properties

In order to study the influence of BS-NPs, as filler, on the vulcanization reaction of SBR

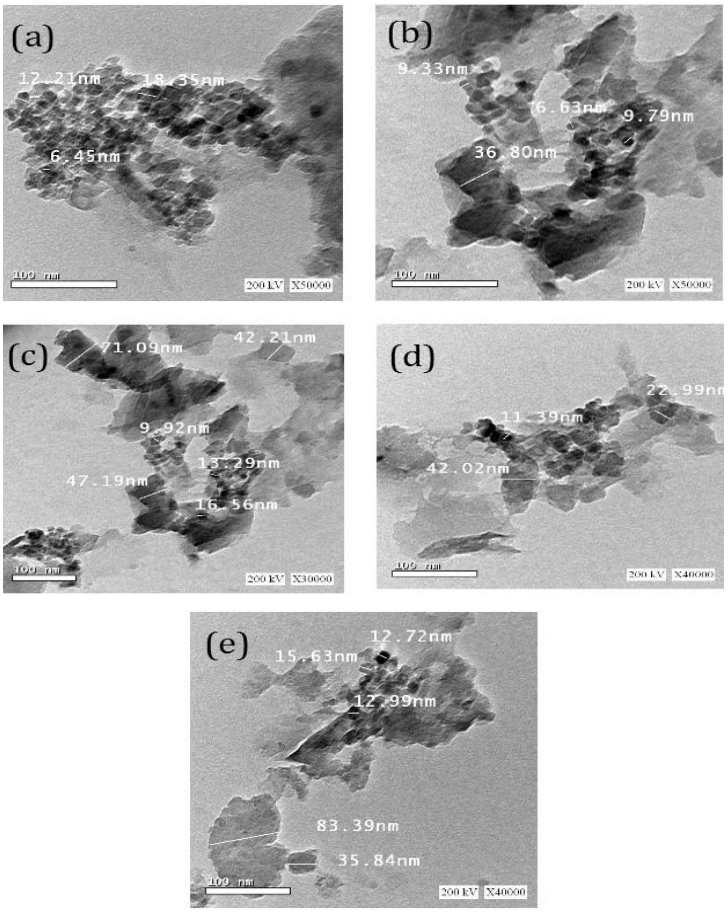

Fig. 2. Transmission electron microscopy analysis of (BS-NPs).

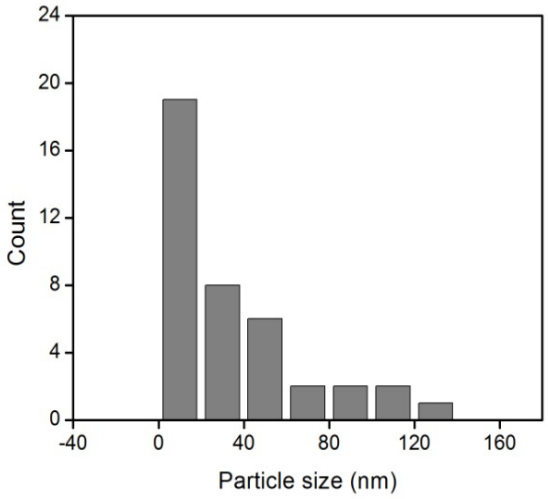

Fig. 3. Histogram of the particle size counts of BS-NPs.

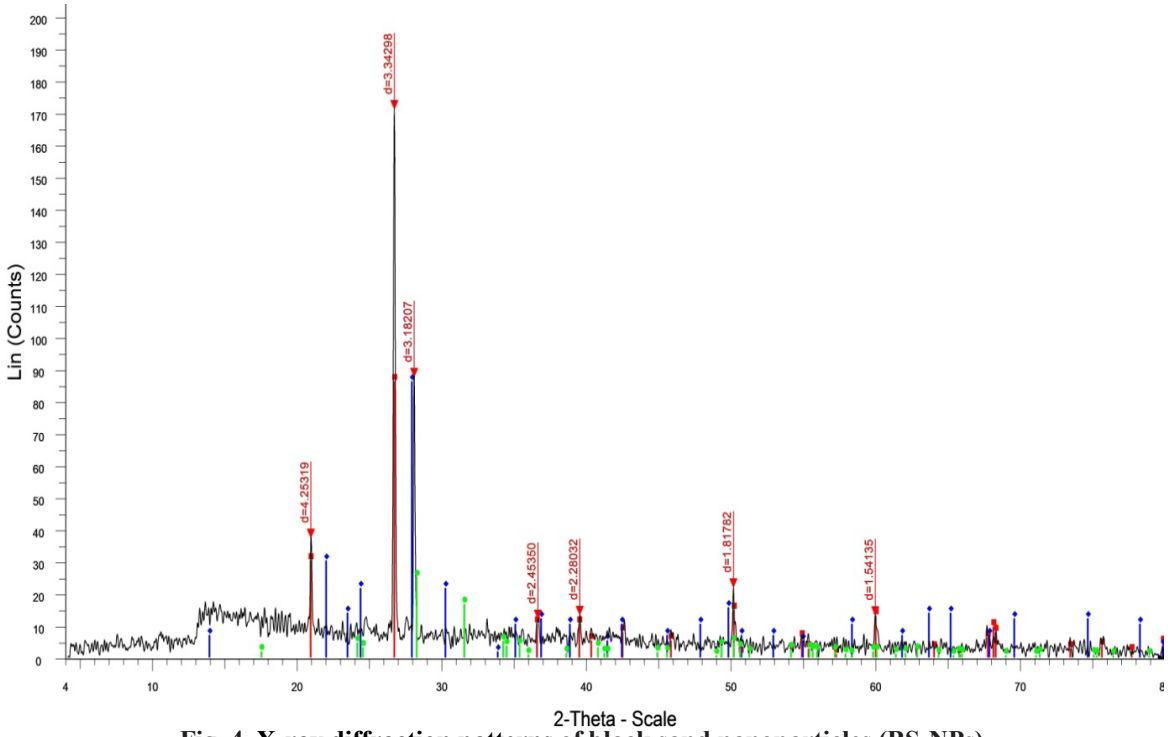

Fig. 4. X-ray diffraction patterns of black sand nanoparticles (BS-NPs).

TABLE 2. Composition of BS-NPs collected from XRD examination.

Mineral name	Chemical structure	Crystallographic phase	Wt, %
Albite (sodium aluminum silicate)	$NaAlSi_3O_8$	Triclinic	63.8
Quartz (silicon dioxide)	SiO_2	Hexagonal	17.7
Baddeleyite (Zirconium oxide)	ZrO_2	Monoclinic	18.5

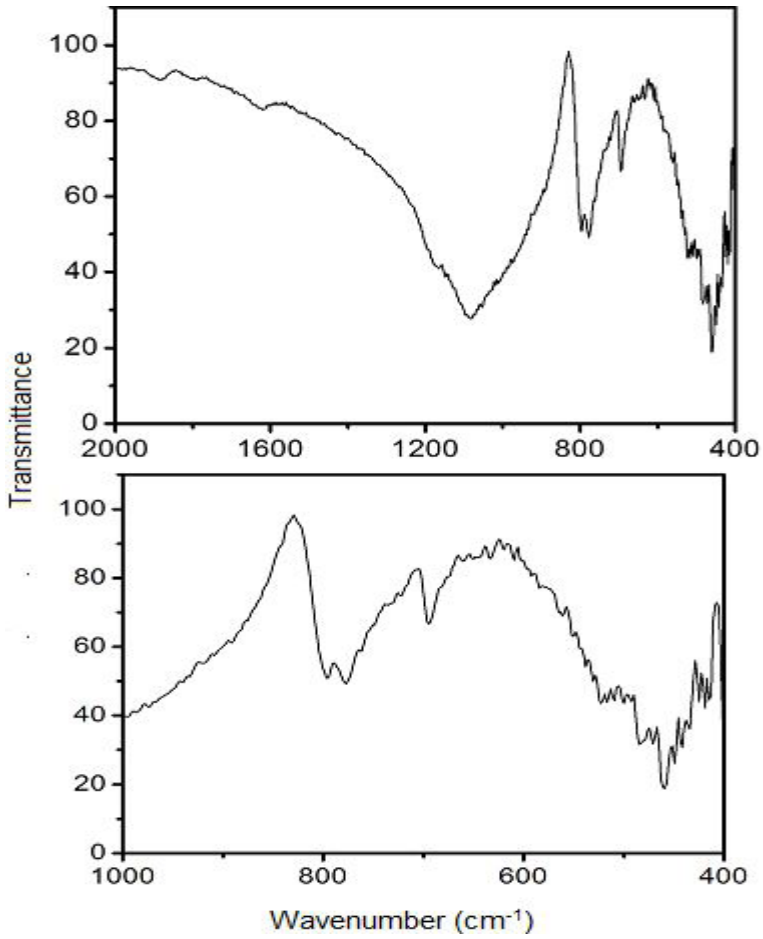

Fig. 5. FT-IR transmission spectra of the black sand nanoparticls (BS-NPs).

compounds, it was interesting to compare the effect of other fillers such as high abrasion furnace black (HAF) and nanosilica (NS) on the SBR composites. The vulcanization curves of samples obtained from oscillating disc rheometer (ODR) were analysed. The rheometric properties of the SBR/nanofillers nanocomposites are given in Table [3]. The results show a decrease of the scorch time (ts_2) value of BR/BS-NPs nanocomposites relative to that of SBR/HAF and SBR/NS nanocomposites. Further decrease in the ts_2 values is observed as the BS-NPs loading increase in the SBR matrix (B4&B5) which indicate a lower scorch safety. The optimum cure time (tc_{90}) defined as the time required to reach 90% of maximum cure. Values of SBR/BS-NPs composites are less than that of SBR/NS and SBR/HAF, at the same filler loadings. As the BS-NPs loadings increase in the composites to 10 and 15 phr the Tc_{90} values decrease indicating that BS-NPs are able to accelerate the vulcanization process of SBR composites. This can be referred to the existence of metal ions such as Zr, Na, Al and Si in the BS-NPs powder which accelerates the curing reaction. The cure rate index (CRI) is a parameter indicates the speed of the curing reaction [16]. At equivalent concentrations of HAF, NS and BS-NPs, samples B1, B2 and B3, the SBR/BS-NPs manifest the highest CRI value. As the BS-NPs loading in the SBR composites increase to 10 and 15 phr, samples B4 and B5, the CRI values increase. This behaviour was reported before to fillers with small surface area that usually speed up the rate of rubber composites curing reaction. It is worthy to mention that Hosseini et al, in a similar study, studied the effect of adding different NSPs loading on SBR nanocomposites in presence of silane coupling agent. Rheological parameters reported by him were much low compared to those obtained in our study specilaay the values of M_L and DM [25]. to These results ensure the outfindings of the morphological studies mentioned previously in section 3.1. The minimum torque (M_L) value represents an index of the material viscosity [26]. From Table [3] we can notice that at equivalent filler concentration of

fillers, the M_L value of SBR/BS-NPs is lower than that of SBR/HAF and SBR/NS. This decrease in the ML value means a decrease in the composites viscosity and in turns an increase in the molecular mobility [26]. This can explain the low Tc_{90} and CRI values of the SBR/BS-NPs composites. The extent of cure (given by ΔM values) decreases in the order B1>B2>B3 containing 5 phr of HAF, NS and BS-NPs respectively. Lower ΔM values was expected for B2 and B3 due to the interaction of the silanol group (-OH), on the silica particles surface, with the accelerator molecules [27]. This deactivating effect of the –OH group leads to a lower ΔM values in comparison to carbon black filled composites (B1). However the reduction of ΔM values of SBR/BS-NPs composites is not dramatic and can be overcome by treating the BS-NPs surface in our future work.

Analysis of the mechanical properties

Table (4) lists the mechanical properties of the SBR nanocomposites. The results of the tensile tests are expressed in terms of the elastic modulus, maximum tensile strength (T.S) and elongation at break percentage (E%). Firstly, we will discuss the effect of 5 phr concentration of HAF, NS and BS-NPs as represented by B1, B2 and B3 respectively. From Table (4) it is clear that B1 showed the highest T.S and elastic modulus values. This result was expected as it was previously reported that nanosilica causes a reduction in the tensile properties when compared to carbon black fillers [28]. This was attributed to the presence of agglomerated nanoparticles that has the tendency for splitting [29]. It is worthy to mention that T.S of SBR/BS-NPs nanocomposite is higher than that of SBR/NS. This result indicates that the degree of dispersion, as well as good interaction in the SBR matrix, is higher for BS-NPs than NS. Another interesting observation is that the lower elastic modulus value of B3 which indicating lower stiffness than B1and B2 nanocomposites. Meanwhile, B3 possess the highest elongation value among B1 and B2. This can be attributed to the reactivity of the BS-NPs due to the existence of quartz (SiO_2), Albite ($NaAlSi_3O_8$) and Baddeleyite (ZrO_2) nanoparticles in it, which can lead to more rubber-filler interaction than filler-filler interaction. Thus the BS-NPs agglomerations do not impede the higher relative deformation of the rubbery matrix. This postulate is evidenced by the highest hardness value exhibited by B3, as hardness value evaluate the resistance of a rubber surface against penetration by an indenter, and relates to the deformation of the rubber surface [30].

The crosslink density

In previous studies, Lawandy et al. [14,15] had successfully used the stress-strain measurements, compression percentage % measurements and ultrasonic measurements to evaluate the crosslink density of rubber compounds. These evaluations were based on the statistical theory of rubber like elasticity[11, 23]. The theory relates the force applied (F) per unit area (A_0) required to strain a perfectly elastic network at a small extension ratio. The compression stress is a reversible process to that of elongation strain. The force applied expressed as F/A_0 for each sample was calculated using Equation (5). Then the calculated F/A_0 was plotted versus $\lambda-\lambda^{-2}$. Consistent linear relations were obtained as shown in Figure (1). The slopes of these straight lines represent $\frac{\rho RT}{Mc}$ value of the samples. Substituting by the values of M_c in Equation (5), the crosslink density of the SBR nanocomposites were obtained, as shown in Figure (6). The experimental procedure and the crosslink density calculations are fully explained above in section 2.4.7. Figure (6) illustrates the crosslink density of the samples containing 5, 10 and 15 phr of BS-NPs together with the control sample and the sample containing 5 phr NS. A dramatic decrease in the crosslink density of rubber vuclanizates is noticed upon adding the nanofillers. Similar behaviour was interpreted before on the basis of the relation between the bound rubber and the crosslink density within the rubber vulcanizates [25]. Bound rubber in rubber vulcanizates is a reinforcement level which is formed by physical bonding between filler and rubber molecules; whereas crosslink density is a level of reinforcement formed during vulcanization between rubber backbone and sulfur, as vulcanizing agent [31,32]. Thus, the decrease in the crosslink density of the SBR rubber composites along with enhancement of mechanical properties, especially elongation at break, indicates a predomination of bound rubber portion. In other words, the active sites on the filler nanoparticles surface compete with the vulcanizing system bonding ability. Another interesting observation, from Figure (6), is that the crosslink density of SBR composites containing 5phr of NS and BS-NPs, samples B3 and B4, are very close to each other. Meanwhile, as the BS-NPs concentration increases in the SBR compounds, samples B4 and B5, the crosslink density slightly decreases.

Conclusion

Black sand (BS) samples were collected from

TABLE 3. Vulcanization characteristics obtained from the rheometer.

Sample	Bo	B1	B2	B3	B4	B5
		SBR/HAF	SBR/NS	SBR/BS-NPs	SBR/ BS-NPs	SBR/ BS-Ps
Property		**5phr**	**5phr**	**5phr**	**10phr**	**15phr**
M_L, Kg.cm	0.37	0.56	0.59	0.52	0.43	0.44
M_H, Kg.cm	5.69	7.91	7.13	6.80	7.06	7.14
D M, Kgm.cm	5.32	7.35	6.54	6.28	6.63	6.70
Scorch time T_{S2}, min	2.20	3.37	3.06	1.52	1.48	1.29
Cure time Tc_{90}, min.	8.52	9.39	10.18	6.37	5.26	5.09
Cure Rate Index, min^{-1}	15.82	16.61	14.04	20.62	26.46	26.32

TABLE 4. Mechanical Properties of the different SBR/filler nanocomposites.

	Nanocomposite	Tensile Strength, MPa	Modulus, MPa	Elongation at break,%	Hardness, Shore A
Bo	SBR	2.04	2.03	335	45.7
B1	SBR/HAF (5phr)	2.74	2.28	416	44.6
B2	SBR/NS(5phr)	2.32	2.18	421	45.3
B3	SBR/ BS-NPs (5phr)	2.57	2	426	45.7
B4	SBR/ BS-NPs (10phr)	1.95	1.95	454	44.4
B5	SBR/ BS-NPs (15phr)	1.84	1.97	377	44.3

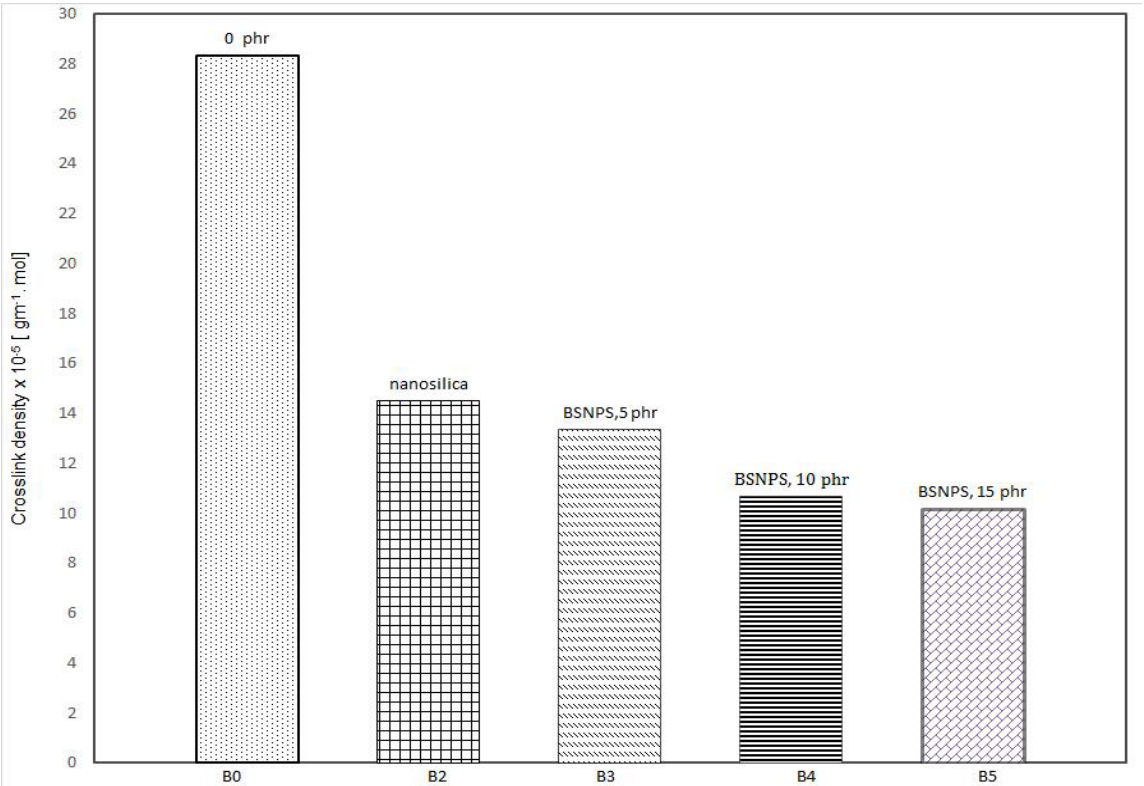

Fig. 6. The crosslink density of SBR control sample, SBR/NS and SBR/BS-NPs nanocomposites containing 5, 10 and 15 phr BS-NPs.

the beach area of Rosetta in Egypt and grinded in a ball milling machine, *an* energy saving and echo-friendly technique, to obtain black sand nanoparticles (BS-NPs). The TEM examination revealed that the milled BS has an average particle size 31nm. The FTIR and XRD examination showed that Black Sand nanoparticles BS-NPs contain quartz (SiO_2), Albite ($NaAlSi_3O_8$) and baddeleyite (ZrO_2) in the ratio 17.7, 63.8 and 18.5 by weight respectively. Results evidenced that the incorporation of BS-NPs in the rubber compounds accelerate the vulcanization reaction as revealed by the lower cure time and higher CRI values relative to that of SBR/NS and SBR/HAF. Also SBR/BS-NPs nanocomposites, even at high concentration, possess lower E-modulus values along with higher E% values. The T.S of SBR/5phr BS-NPs was higher than that of SBR/NS nanocomposites. The study of the crosslink density values of SBR/NS and SBR/BS-NPs nanocomposites shed light on the type of bonds in the SBR/BS-NPs. The decrease in the crosslink density values of the SBR/BS-NPs, relative to that of SBR/ HAF and SBR/NS nanocomposites, without scarifying E% values evidenced a higher adhesion of the rubber matrix to the BS-NPs surface.

References

1. Yazdimamaghani, M. et al. 'Synthesis and Characterization of Encapsulated Nanosilica Particles with an Acrylic Copolymer by in Situ Eteriamulsion Polymerization Using Thermoresponsive Nonionic Surfactant', Materials, Vol. 6 No. 9,pp.3727-41 (2013).
2. Lee, J. et al. 'Synthesis of polystyrene/silica composite particles by soap-free emulsion polymerization using positively charged colloidal silica', *J. Colloid & Inter. Sci*., Vol. 310 No. 1, pp.112–120 (2007).
3. Lin, M. et al. 'Silicone–polyacrylate composite latex particles, particles formation and film properties', *Polymer*, Vol. 46 No. 4, pp.1331-37 (2005).
4. Abdel-Karim, A. M. and El-Shafey, A. M. 'Mineralogy and chemical distribution study of placer cassiterite and some associated new recorded minerals, east Rosetta, Egypt', *Arabian Journal of Geoscience*, Vol. 5 No. 4, pp.807–816 (2012).
5. Dabbour, G. A. 'Estimation of the economic minerals reserves in Rosetta beach sands', *Egyptian Minerals*, Vol. **7**, pp.1-6 (1995).
6. El-Shazly, E. M. and Wassef, S. 'Statistical relation reflecting the depositional environment of east Rosetta beach sands', *Egyt. Journal of Geology*, Vol. 26 No. 1, pp.1–19 (1982).
7. Dabbour, G. A., In Proceedings of The *2nd. Arab Conference on the Peaceful Uses of Atomic Energy*, 'The Egyptian placer deposits: a potential source for nuclear raw materials', paper presented at. 5-9 Nov 1994. Cairo, Egypt.
8. Wassef, S. N. 'Distribution and properties of placer ilmenite in east Rosetta beach sands', *Egyt. Mineralium Deposita*, Vol. 16, pp.259–267 (1981).
9. El-Askary, M. A. and Frihy, O. E. 'Depositional phases of Rosetta and Damietta promontories on the Nile delta coast', *Egyt. J. Afri Earth Sci*., Vol. 5 No. 6, pp.627-633 (1987).
10. Mahmoud, H. H. et al. 'Distribution of Some Elements in the Egyptian Black Sands from Abu Khashaba Beach Area', *J. Anal. Sci. Math. & Instr*., Vol. 3, pp.62-66 (2013).
11. Guo, G.Y. and Chen, Y. L. 'Unusual structural phase transition in nanocrystalline zirconia', *Appl. Phys. A*, Vol. 84 No. 4, pp. 431-437 (2006).
12. Delogu, F. et al. 'Fabrication of polymer nanocomposites via ball milling: Present status and future perspectives', *Prog. Mater. Sci*., Vol. 86, pp.75–126 (2017).
13. Mio, H. et al. 'Scale-up method of planetary ball mill', *Chem. Eng. Sci*., Vol.59 No. 24, pp.5909–5916 (2004).
14. Lawandy, S. N. et al. 'Ultrasonic and Mechanical Measurements for the Detection of Crosslink Density of SBR and NBR Based on Various Curing Systems', *J. Appl. Polym. Sci*. Vol. 112 No.1, pp.366–371 (2009).
15. Lawandy, S. N. and Halim, SF 'Effect of vulcanizing system on the crosslink density of nitrile rubber compounds', *J. Appl. Polym. Sci*. Vol. 96, pp.2440 –2445 (2005).
16. Biagiotti, J. et al. 'Cure characteristics, mechanical properties, and morphological studies of linoleum flour-filled NBR compounds', *Polym. Eng. Sci*., Vol. 44 No. 5, pp.909-916 (2004).
17. Nanda, K. K. et al. 'Higher surface energy of free nanoparticles', *Phys. Rev. Lett.*, Vol. 92 No. 17,

pp.1-4 (2004).

18. Zhou, Z. Y. et al. 'Nanomaterials of high surface energy with exceptional properties in catalysis and energy storage', *Chem. Soc. Rev*., Vol. 40 No. 7, pp. 4167-41 (2011).

19. Seah, K. H. W. et al. 'Mechanical properties of cast aluminium alloy 6061–albite particulate composites', Proceedings of the Institution of Mechanical Engineers Part I, *J. Mat. Des. Appl*., Vol. 214, pp. 1-6 (2000).

20. Salami-Kalajahi, M. et al. 'Study of kinetics and properties of polystyrene/silica nanocomposites prepared via in situ free radical and reversible addition-fragmentation chain transfer polymerizations', *Scientia Iranica*., Vol. 19 No. 6, pp.2004–2011 (2012).

21. Söderlund, U. and Johansson, L. 'A simple way to extract baddeleyite (ZrO2)', *Geochem Geophys Geosys*, Vol. 3 No. 2, pp. 1-7 (2002).

22. Sivakumar, S. et al. 'FTIR Spectroscopic Studies on Coastal Sediment Samples from Cuddalore District, Tamilnadu, India', *Indin J. Adv. Chemi. Sci*., Vol. 1, pp. 40-46 (2012).

23. Ritz, M. et al. 'Determination of chlorite, muscovite, albite and quartz in claystone and clay shales by infrared spectroscopy and partial least-squares regression', *Acta Geodyn Geomater*, Vol. 9 No. 4, pp.511–520 (2012).

24. Chen, S. G. et al. 'Structures, growth modes and spectroscopic properties of small zirconia clusters', *J. Crysl. Growth*, Vol. 282 No. 3-4, pp.498-505 (2005).

25. Hosseini, S. M. and Razzaghi-Kashani, M. 'Vulcanization kinetics of nano-silica filled styrene butadiene rubber', *Polymer*, Vol. 55 No. 24, pp.6426-6434 (2014).

26. Hasan, A. et al. 'Rubber mixing process and its relationship with bound rubber and crosslink density', Paper presented at the *IOP Conference Series: Materials Science and Engineering*. 23-25 May 2017. Guangzhou, China (2017).

27. Coran A. Y. '*Science and Technology of rubber*', New York: Academic Press, Chapter 7, Vulcanization; pp.291-338 (1978).

28. Liu, Y. and Kontopoulou, M. 'The structure and physical properties of polypropylene and thermoplastic olefin nanocomposites containing nanosilica', *Polymer*, Vol. 47 No. 22, pp.7731-7739 (2006).

29. Li, J. X. et al. 'The ductile-to-quasi-brittle transition of particulate-filled thermoplastic polyester', *J. Appl. Polym. Sci.,* Vol. 52 No. 2, pp.255-267 (1994).

30. Yan, F. et al. 'Adjusting the properties of silicone rubber filled with nanosilica by changing the surface organic groups of nanosilica', *Composites Part B Eng.*, Vol. 75, pp.47-52 (2015).

31. Billmeyer, F. W. '*Textbook of Polymer Science, 3rd ed*', John Wiley & Sons, New York, pp.578 (1984).

32. Morton, M. '*Rubber Technology*', New York: Springer Science and Business Media Dordrecht (1997).

الإستفادة من جزيئات الرمل الأسود النانومترية كمادة مالئة لمتراكبات مطاط إستيرين بيوتاداين

سمير نجيب لاوندي[١]، رانيا سيد أحمد[٢]، بسمة كمال صالح[١] و سوسن فخري حليم[١]

[١]معمل مترولوجيا وتكنولوجيا البوليمرات - المعهد القومي للمعايرة - مصر.

[٢]معمل تكنولوجيا ومترولوجيا النانو - المعهد القومي للمعايرة - مصر.

يتوافر الرمل الأسود بكثرة على شواطئ الروزيتا في جمهورية مصر العربية، وقد تم الحصول عليه من هذه الشواطئ وطحنها للحصول على جزيئات الرمل الأسود النانومترية ""BS-NPs وتوصيفها بأحدث التقنيات مثل XRD TEM. أظهرت نتائج XRD أن هذه الجزيئات النانومترية تتكون أساساً من الأبيت (سيليكات الألومنيوم الصوديومي) بنسبة تصل إلى ٦٤ ٪، بينما تصل نسبتي ثاني أكسيد السيليكون وأكسيد الزركونيوم إلى ١٧,٧ و ١٨,٥ ٪ على الترتيب. يتراوح حجم جزيئات الرمل الأسود النانونية - وفقاً لنتائج تحليل TEM – من ٦ إلى ١٢٢ ن م بمتوسط قطر ٣١ نانومتر. وقد تم إضافة BS-NPs كمادة مالئة إلى خلطات مطاط الإستيرين البيوتيلي ودراسة الخواص الريومترية والميكانيكية للمتراكبات الناتجة ومقارنة النتائج بمثيلاتها المحضرة بإستخدام أسود الكربون و السيليكا ا النانومترية. وقد أوضحت النتائج تقارب نتائج القياسات الريومترية والميكانيكية لمتراكبات الرمل الأسود النانومترية بمثيلانها للمتراكبات المحضرة بإستخدام السيلسكا النانومترية.